SIAM J. Applied Dynamical Systems
Vol. 2, No. 2, pp. 238–253
© 2003 Society for Industrial and Applied Mathematics

Predicting Irregularities in Population Cycles*

Shandelle M. Henson†, James R. Reilly‡, Suzanne L. Robertson§, Matthew C. Schu§, Eric W. D. Rozier§, and J. M. Cushing¶

Abstract. Oscillating population data often exhibit cycle irregularities such as episodes of damped oscillation and abrupt changes of cycle phase. The prediction of such irregularities is of interest in applications ranging from food production to wildlife management. We use concepts from dynamical systems theory to present a model-based method for quantifying the risk of impending cycle irregularity.

Key words. nonlinear population dynamics, stochasticity, periodic solutions, phase switching, basins of attraction

AMS subject classifications. 39A11, 92D25

PII. S1111111102411262

1. Introduction.

Animal numbers can oscillate periodically in many biological populations. Laboratory examples include paramecia [22], blowflies [33], bean weevils [37], moths [3], and flour beetles [6, 19].

Noise, always present in population dynamics, causes cycle irregularities such as outbreaks, switches in oscillation phase [28], and episodes of damped oscillations caused by "saddle fly-bys" [11] or other stochastic visitations of unstable equilibria. Phase switches (when, for example, an "up-down" time series pattern becomes a "down-up" pattern) occur rather frequently in laboratory populations of the flour beetle *Tribolium castaneum*. Figure 1.1 displays the larval numbers from control B of the experiment reported in Desharnais and Costantino [16]. The data oscillate with period two but switch cycle phase at times $t = 3$ and $t = 13$.

Cycle irregularities are important in a variety of applications ranging from food production to forest management to species conservation. In this paper, we use the concepts of dynamical systems theory to devise a method for predicting such irregularities in oscillating data.

In section 2, we use the univariate Ricker map to illustrate the dynamic mechanisms that give rise to cycle irregularities and to develop a method for predicting such irregularities. Section 3 applies the theoretical ideas to simulated data sets generated by two different multivariate models. In section 4 we use the method to predict cycle irregularities in experimental data replicates of laboratory cultures of the flour beetle *Tribolium*.

*Received by the editors July 16, 2002; accepted for publication (in revised form) by G. B. Ermentrout February 20, 2003; published electronically May 23, 2003. This work was supported in part by the National Science Foundation (Cushing, Henson), a Howard Hughes Medical Institute grant to the College of William and Mary (Henson, Reilly, Rozier, Schu), a U. S. Charles Center Summer Research Scholarship (Reilly), and a Verizon Scholarship (Robertson).
http://www.siam.org/journals/siads/2-2/41126,html
†Department of Mathematics, Andrews University, Berrien Springs, MI 49104 (henson@andrews.edu).
‡Department of Entomology, Cornell University, Ithaca, NY 14850 (jrr28@cornell.edu).
§College of William and Mary, Williamsburg, VA 23187 (slrobe@wm.edu, mcschu@wm.edu, ewdavi@wm.edu).
¶Department of Mathematics, University of Arizona, Tucson, AZ 85721 (cushing@math.arizona.edu).

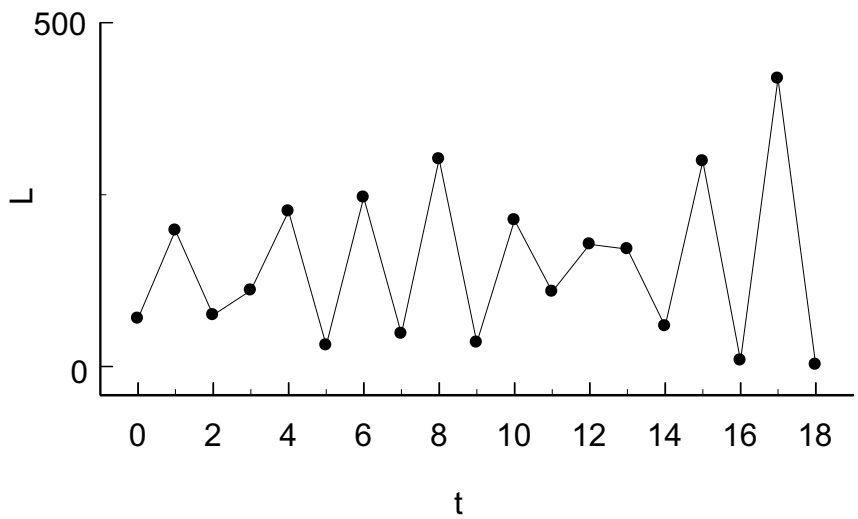

Figure 1.1. *Experimental data from Desharnais and Costantino* [16] *replicate B.* Tribolium castaneum *larval numbers oscillate in a* 2*-cycle. Phase switches occur at times* $t = 3$ *and* $t = 13$*. The time step is two weeks.*

2. Cycle irregularities. Consider a discrete time autonomous population model of the form $x_{t+1} = f(x_t)$ where x is a scalar, a vector of life stage classes, or a vector of interacting populations. To illustrate these ideas, consider specifically the scalar Ricker population model [31, 32, 34]

$$x_{t+1} = bx_t e^{-cx_t}. \tag{2.1}$$

The Ricker map (2.1) has stable periodic solutions at many values of its parameters. For example, when $b = 9$ and $c = 1$, the Ricker map has a stable 2-cycle solution given by $x_0 = 1.099$, $x_1 = 3.296$, $x_2 = 1.099$, $x_3 = 3.296, \ldots$. Since (2.1) is autonomous, the phase shift $x_0 = 3.296$, $x_1 = 1.099$, $x_2 = 3.296$, $x_3 = 1.099$, $\ldots$ is also a stable 2-cycle solution. Denote the first cycle "Phase 1" and the second "Phase 2." Let B_1 be the set of positive initial conditions $x_0 \in R^+$ that give rise to solutions converging to the Phase 1 cycle, and let B_2 be the set of positive initial conditions that give rise to solutions converging to Phase 2. These "basins of attraction" for the two cycle phases are sets on the real line. Some of the numerically computed boundaries separating these phase basins are shown in Figure 2.1(a). Initial conditions x_0 with $4.840 < x_0 < 7.425$ converge to Phase 1; initial conditions with $2.198 < x_0 < 4.840$ converge to Phase 2; those with $0.345 < x_0 < 2.198$ converge to Phase 1; those with $0.040 < x_0 < 0.345$ converge to Phase 2; and so forth. (Near the origin, the basin structure becomes complicated and cannot be shown in Figure 2.1(a).) Note that the unstable equilibrium $x_u = 2.198$ lies on the basin boundary. The reader should also note that

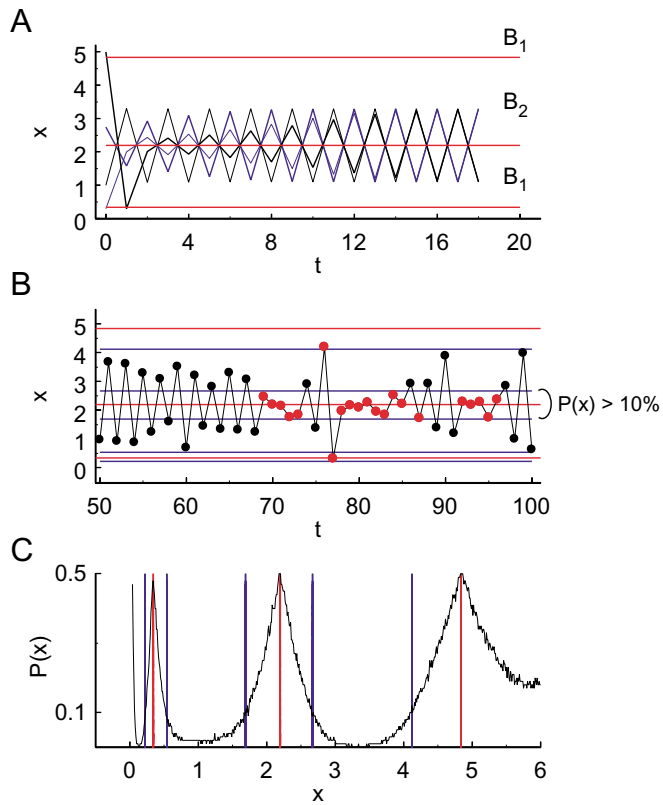

Figure 2.1. *Ricker map simulations with $b = 9$ and $c = 1$.* (a) *Four deterministic Ricker time series with initial conditions $x_0 = 0.3$, $x_0 = 1$, $x_0 = 2.75$, and $x_0 = 5$. Red horizontal lines represent basin boundaries at $x = 0.3445$, $x = 2.198$, and $x = 4.840$. Since $x_0 = 1$ and $x_0 = 5$ are both in basin B_1, their orbits converge to Phase 1 (shown in black). Since $x_0 = 0.3$ and $x_0 = 2.75$ are both in basin B_2, their orbits converge to Phase 2 (shown in blue).* (b) *Stochastic Ricker simulation with $\sigma^2 = 0.0225$. Red horizontal lines represent basin boundaries as in* (a)*. The red lines are bracketed by blue horizontal lines that demarcate the 10% zones. Points on the orbit which lie in the 10% zones are colored red and have at least a 10% probability of switching phase at the next time step.* (c) *The probability $P(x)$ of switching phase at the next time step given the current value of x. Red vertical lines represent values of x at which $P(x) = 50\%$ and correspond to the basin boundaries. Blue vertical lines show values of x at which $P(x) = 10\%$ and correspond to the boundaries of the 10% zones.*

the term "basin" is being used here to differentiate two separate basins of attraction for two different solutions lying on the same 2-cycle attractor, while the usual meaning lumps B_1 and B_2 together as a single basin of attraction for the 2-cycle attractor itself. (To view B_1 and B_2 as basins in the traditional sense, we could use the composite map to decompose the 2-cycle attractor into two separate stable equilibria with two separate basins of attraction. However, this complication is unnecessary for our purposes.)

If $x_0 \in B_1$ so that the solution converges to Phase 1, then taking $f(x_0)$ as an initial condition would lead to a solution converging to Phase 2; hence $x_1 = f(x_0) \in B_2$. Similarly,

if $x_0 \in B_2$, then $x_1 \in B_1$. In this way, deterministic orbits must always bounce back and forth between the two basins at each time step as they converge to the appropriate phase of the 2-cycle (Figure 2.1(a)).

Process noise in ecological data is of two basic types: environmental and demographic. Environmental noise is additive on the log scale, while demographic noise is additive on the square root scale [15]. The methods in this paper work equally well for both kinds of noise; however, we will focus on demographic stochasticity. Thus we can incorporate demographic noise by means of

$$x_{t+1} = \left(\sqrt{bx_t e^{-cx_t}} + E_t\right)^2, \tag{2.2}$$

where E_t is a random normal variable with mean zero and variance σ^2 (see Dennis et al. [15]). When $\sigma = 0$, we recover the "deterministic skeleton" (2.1) [36]. As σ increases from zero, the cycles become irregular. In particular, orbits may not always alternate between basins at each time step. If a stochastic orbit remains in the same basin for two consecutive time steps, we say a "phase switch" has occurred. For example, in the stochastic simulation shown in Figure 2.1(b), the orbit is in Phase 2 for $t = 86$ to 91 but in Phase 1 for $t = 97$ to 100. On examination of the basins in which the $t = 92$ to 96 values lie, we see that the orbit switches phase at $t = 97$, since x_{96} and x_{97} are both in B_2.

The conditional probability $P(x)$ of switching phase at the next time step, given a current value of x, is graphed in Figure 2.1(c). $P(x)$ is lowest at the 2-cycle values $x = 1.099$ and $x = 3.296$ and is highest along the basin boundary. $P(x)$ can be considered a kind of measure of how far a point is from the deterministic attractor or, alternately, how close a point is to the basin boundary.

Figures 2.1(b) and (c) show the numerically computed values of x for which $P(x) = 10\%$. These values bracket the basin boundaries; and when x falls inside these "10% zones," there is at least a 10% chance of suffering a phase switch at the next time step. For example, $P(x) > 10\%$ whenever $1.691 < x < 2.669$.

For the stochastic orbit in Figure 2.1(b), all values x_t for which $P(x_t) \geq 10\%$ are colored red. Note how the red tagging provides a fairly good warning of impending cycle irregularities. For example, at $t = 69$, the orbit falls into a 10% zone, and the following values for $t = 70$ to 73 are highly irregular. At $t = 76$ the orbit again enters the 10% zone, and irregularities follow for $t = 77$ to 85. At $t = 92$ the orbit once more lands in the 10% zone, and irregularities, including the aforementioned phase switch at $t = 97$, follow.

Note how the orbit sometimes lingers near the unstable equilibrium $x_u = 2.198$ if stochastically bumped into its vicinity (for example, at times $t = 70, 79, 92$). This phenomenon is similar to a "saddle fly-by," although the unstable equilibrium here is a repellor rather than a saddle. In a "saddle fly-by," the orbit is stochastically bumped near the stable manifold of a saddle and approaches the saddle before moving away. In a "repellor visitation," the orbit is stochastically knocked directly into the neighborhood of a repellor or maps in from a nonlocal stable set and then lingers before moving away. In cycling data, saddle fly-bys and repellor visitations of unstable equilibria typically give rise to episodes of damped oscillation [11].

To summarize this example, we suggest an empirical "rule of thumb":

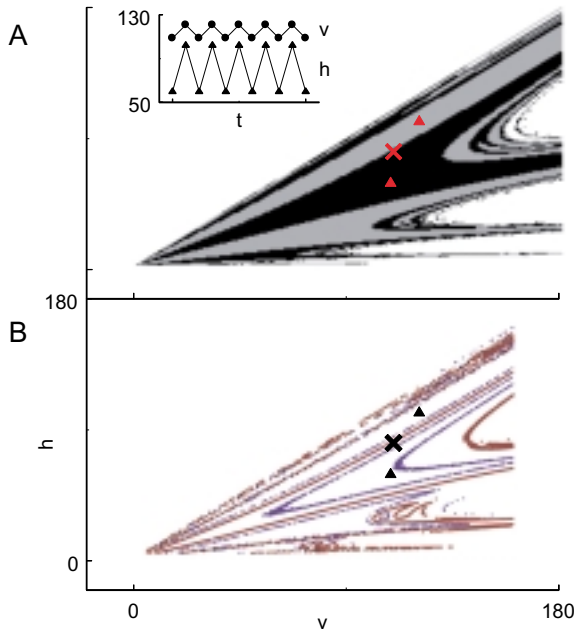

Figure 3.1. *Leaf-herbivore model simulations with $f = 1.5$, $a = .005$, $r = 3.8$, and $\delta = 1.0$.* (a) *Basins of attraction for the two phases of the attracting 2-cycle. The basins were determined by iterating points in state space (on a grid of mesh $1/10$) forward 200 time steps with the deterministic model. The red triangles are the 2-cycle values $(v, h) = (108.76, 59.94)$, $(120.9, 102.25)$. The unstable saddle equilibrium $(v, h) = (110, 81)$ is indicated by a red "x." The 2-cycle attractor is shown above this plot as a time series.* (b) *Approximation of the 50% (red) and 10% (blue) contour lines for $P(v, h)$. These curves were computed by finding the frequency of phase switching at the next step for points on a grid of mesh $1/10$ in state space. Each point tested was iterated one time step forward, 2000 times, with $\sigma_v^2 = .008$ and $\sigma_h^2 = .032$. The set of all initial conditions with $9.75\% - 10.25\%$ probability of switching phase on the next step is plotted in blue. The set of all initial conditions with $49.5\% - 50.5\%$ probability of switching phase on the next step is plotted in red. The deterministic 2-cycle values are indicated by triangles and the unstable equilibrium by an "x."*

Remark 2.1. *The conditional probability $P(x)$ of switching phase at the next time step, given a current data point x, can be considered a measure of how close the point x is to the basin boundary. The set of points for which $P(x) \geq 10\%$ brackets the basin boundaries. When the current data point falls within these "10% zones," cycle irregularities are likely to follow. The choice of 10% is subjective and depends on the acceptable risk level in the particular application. A more conservative approach would use a smaller contour value (and hence a wider zone around the basin boundaries).*

3. Theoretical examples in population models.

In this section, we use two examples to illustrate how cycle irregularities occur in multivariate models and in cycles of periods other than 2. The first example is a two-species model with a 2-cycle, and the second is a single species structured model with a 4-cycle.

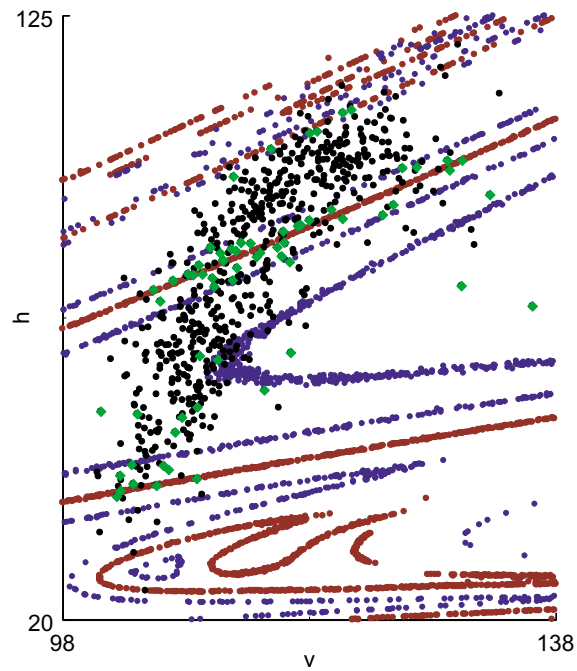

Figure 3.2. *Stochastic orbit of the leaf-herbivore model with* $\sigma_v^2 = .008$ *and* $\sigma_h^2 = .032$. 600 *time steps are plotted in a close-up of state space. Red curves approximate basin boundaries; blue curves bracket the basin boundaries and demarcate the* 10% *zones. Points of the orbit that suffered a phase switch at the next step are colored green; note that most lie within the* 10% *zones, as expected.*

3.1. Leaf-herbivore model. Consider a leaf-herbivore model of Edelstein-Keshet [20],

$$\begin{aligned} v_{t+1} &= f e^{-a h_t} v_t, \\ h_{t+1} &= r\left(\delta - \frac{h_t}{v_t}\right) h_t, \quad v_t \neq 0, \end{aligned} \tag{3.1}$$

where h_t is the number of herbivores at time t on a tree of leaf mass v_t and f, a, r, and δ are positive constants. When $f = 1.5$, $a = 0.005$, $r = 3.8$, and $\delta = 1$, this model has a stable 2-cycle attractor, both phases of which are stable solutions. The basins of attraction for the two phases are shown in Figure 3.1(a), along with the 2-cycle values and an unstable saddle equilibrium lying on the basin boundary.

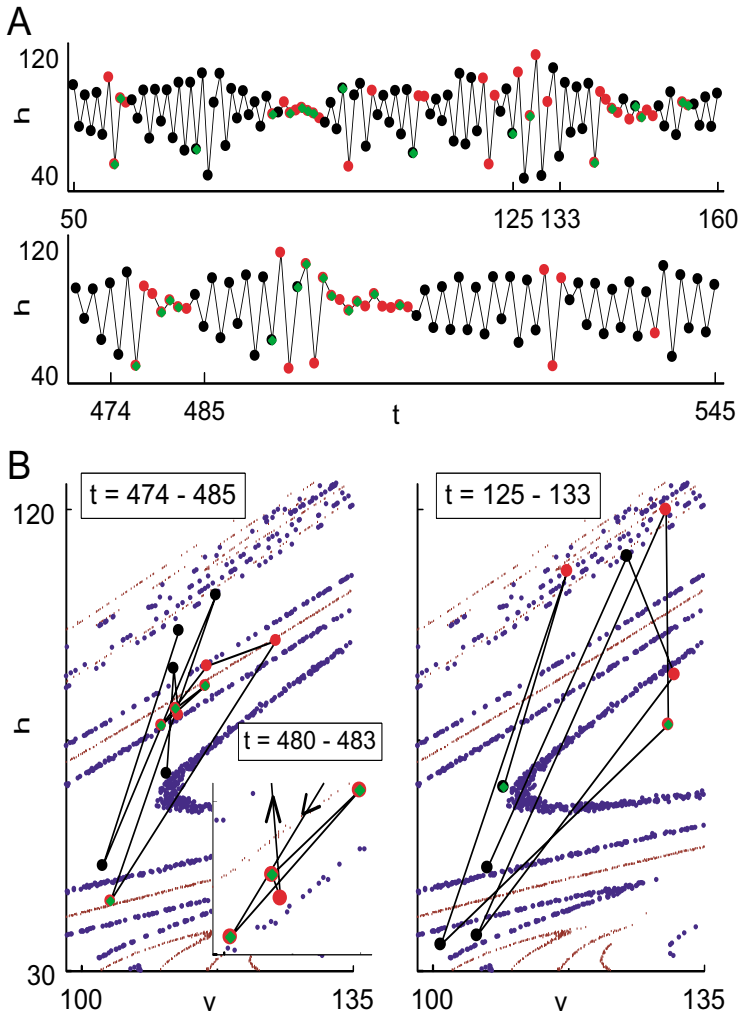

Figure 3.3. *Stochastic orbit of the leaf-herbivore model with* $\sigma_v^2 = .008$ *and* $\sigma_h^2 = .032$. *Points on the orbit that fall within the* 10% *zones are colored red. Points that suffered a phase change at the next time step are indicated by a green diamond.* (a) *h component for two sections of the stochastic time series shown in Figure* 3.2. *Two typical kinds of cycle irregularities are contained in sections* $t = 125$ *to* 133 *and* $t = 474$ *to* 485. *In the first case, the oscillations are irregular (down-up-up) with large amplitude, while in the second case the oscillations are irregular and damped.* (b) *State space close-ups of two sections of the time series in* (a). *For* $t = 474$ *to* 485, *the orbit starts out regularly, following the deterministic* 2*-cycle. Beginning at* $t = 477$, *the orbit lands near the basin boundary, then switches phase, and lands near the basin boundary again. From there the orbit follows the stable manifold toward the unstable equilibrium for a saddle fly-by before returning to the* 2*-cycle. A close-up of the saddle fly-by is shown for* $t = 480$ *to* 483. *The panel for* $t = 125$ *to* 133 *shows how the orbit is knocked far from the* 2*-cycle and visits regions of state space in which the basins are more complicated.*

Consider the stochastic model

$$v_{t+1} = \left(\sqrt{fe^{-ah_t}v_t} + E_{1t}\right)^2, \tag{3.2}$$
$$h_{t+1} = \left(\sqrt{r\left(\delta - \frac{h_t}{v_t}\right)h_t} + E_{2t}\right)^2, \quad v_t \neq 0,$$

where the random vector $\mathbf{E}_t = (E_{1t}, E_{2t})'$ is assumed to have bivariate normal distribution with mean vector $\mathbf{0}$ and variance-covariance matrix $\mathbf{\Sigma}$ [15].

Given that the stochastic system (3.2) is at (v_t, h_t) in state space, one can numerically compute the probability $P(v_t, h_t)$ that the next stochastic step (v_{t+1}, h_{t+1}) will be a phase switch. Figure 3.1(b) shows two numerically computed contours in state space along which $P(v, h)$ is constant. Along the blue contours, $P(v, h) = 10\%$, and along the red contours, $P(v, h) = 50\%$. Note that the 50% contours follow the basin boundaries, while the 10% contours roughly parallel and "bracket" the boundaries. We will call these bracketing sets "10% zones."

Figure 3.2 shows a stochastic run of 600 time steps in a close-up of the state space plot shown in Figure 3.1(b). The orbit points which suffer a phase switch at the next step are green. Note that most of the green points lie within the 10% zones. Indeed, less than 10% of all points landing outside the 10% zones are expected to give rise to phase switches at the next step. By their definition, the 10% zones give a fairly accurate indication of impending phase switches.

Do the 10% zones also provide a good indicator for the onset of other types of cycle irregularities? In Figure 3.3, we consider two sections of the stochastic time series of Figure 3.2. Orbit points landing within the 10% zones are colored red, while those leading to phase switches are also marked by a green diamond. Two typical kinds of cycle irregularities appear in the sections $t = 125$ to 133 and $t = 474$ to 485 (Figure 3.3(a)). In the first case the time series oscillations are irregular ("down-up-up") with large amplitude, while in the second case the oscillations are irregular and damped. In Figure 3.3(b), we take a closer look in state space at the mechanics of these time series irregularities. The section beginning with $t = 474$ starts off with a fairly regular pattern, following the deterministic 2-cycle. At $t = 477$, the orbit lands near the basin boundary within the 10% zone, then switches phase, and lands near the basin boundary again. From there the orbit follows the stable manifold toward the unstable equilibrium and lingers for a saddle fly-by before returning to the 2-cycle. The section beginning with $t = 125$ starts with a point outside the 10% zone but which in fact leads to an unpredicted phase switch. The next step ($t = 126$) is, however, inside the 10% zone, even though in the time series it appears rather unremarkable (Figure 3.3(a)). Although there is no phase switch at the next step, there is an upcoming irregularity. The orbit is stochastically knocked down across three basin boundaries and then to the right into a 10% zone, after which it switches phase and lands far from the attractor. A similar pattern follows until the orbit lands outside the 10% zone fairly close to the attractor at $t = 133$, after which the pattern becomes more regular.

In both of these cases of irregularity, a 10% zone visitation (at $t = 477$ and $t = 126$) served as a warning of the upcoming cycle disturbance. Furthermore, in both cases, the

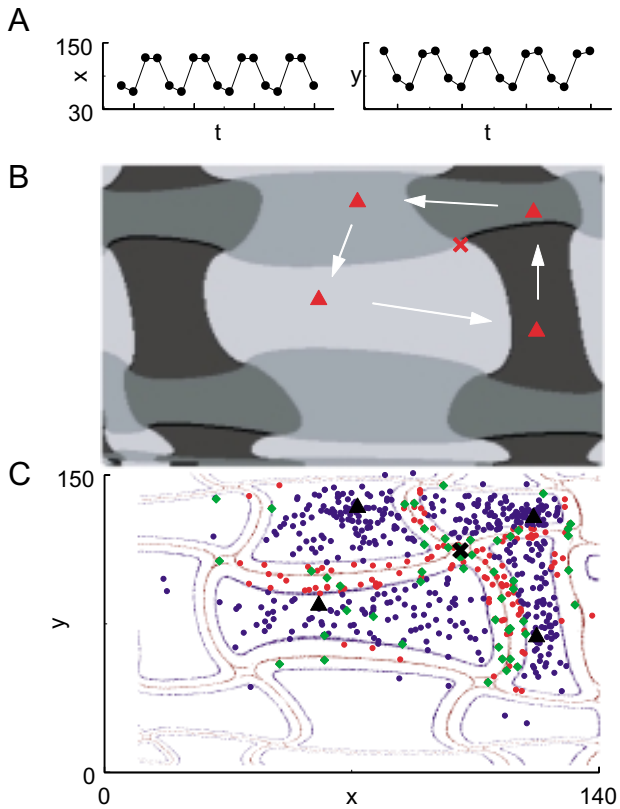

Figure 3.4. *Bartlett model simulations with* $\alpha = 0.02$, $b = 3.14$, *and* $\mu = 0.9$. (a) *Time series for Bartlett model* 4*-cycle.* (b) *Four basins of attraction corresponding to the four phases of the attracting* 4*-cycle. The* 4*-cycle values, indicated by red triangles, are* $(x, y) = (60.67, 85.09)$, $(122.38, 69.18)$, $(121.51, 129.30)$, $(71.64, 133.44)$. *White arrows show the temporal sequence. The red "x" marks the unstable equilibrium at* $(x, y) = (100.80, 112.00)$. (c) 50% *and* 10% *contour lines of* $P(x, y)$ *for the stochastic Bartlett model are represented by red and blue curves, respectively. Here* $\sigma_x^2 = 0.045$ *and* $\sigma_y^2 = 0.025$. *To compute the phase switching frequency,* 2000 *one-step stochastic predictions were made from each point on a grid of mesh* 1/10. *Also shown is a* 600 *step stochastic orbit. Points landing within the* 10% *zone are colored red. Orbit points that switched phase at the next step are indicated by green diamonds. Black triangles mark the values of the deterministic* 4*-cycle, while a black "x" identifies the unstable equilibrium.*

crucial orbit point (at $t = 477$ and $t = 126$) would appear unremarkable in the unfolding time series (Figure 3.3(a)) unless one had knowledge of its proximity in state space to the basin boundary as measured by the 10% zone or some other appropriate measure.

3.2. Bartlett model. In this example, we consider a well-known juvenile-adult model of Bartlett [1]. A stochastic version is

$$x_{t+1} = \left(\sqrt{(b - \alpha y_t)\, y_t} + E_{1t}\right)^2, \tag{3.3}$$
$$y_{t+1} = \left(\sqrt{x_t + (1 - \mu)\, y_t} + E_{2t}\right)^2,$$

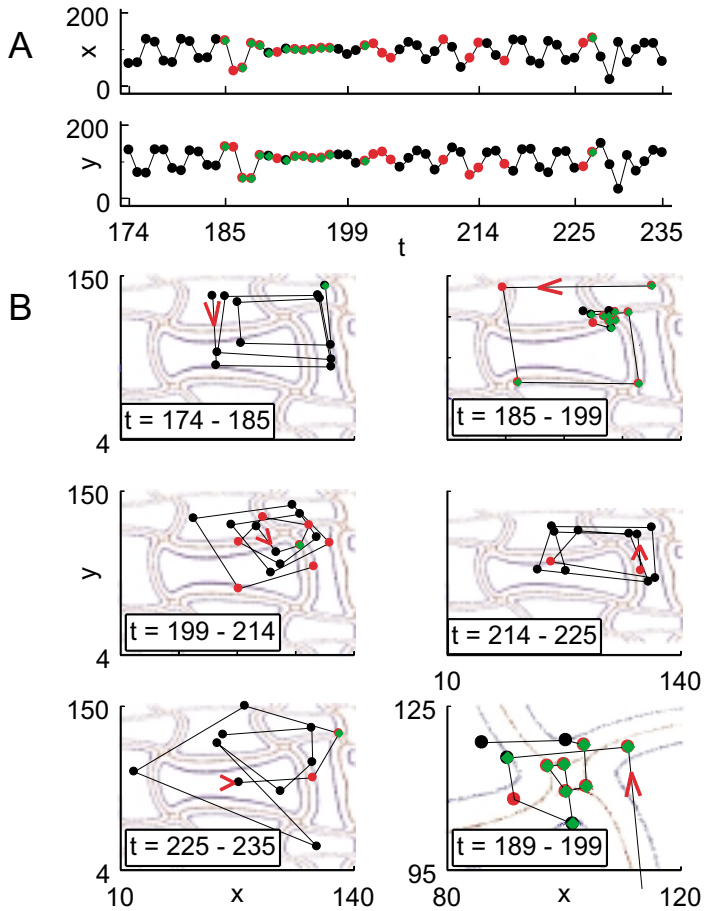

Figure 3.5. *Stochastic simulation of Bartlett model with* $\alpha = 0.02$, $b = 3.14$, $\mu = 0.9$, $\sigma_x^2 = 0.045$, *and* $\sigma_y^2 = 0.025$ *from Figure* 3.4(c). *Orbit points falling within the* 10% *zone are colored red. Green diamonds indicate points that lead to a phase switch at the next time step.* (a) *The time series is divided into five sections of interest (see text).* (b) *State space graphs of the five sections of the stochastic time series in* (a). 50% *and* 10% *contour lines for* $P(x, y)$ *are shown in red and blue, respectively. Orbit points are shown in temporal sequence, with the direction of motion indicated by red arrows.* $t = 174$ *to* 185 *shows a fairly regular section, but we see in state space that the last orbit point is within a* 10% *zone and in fact leads to a phase switch at the next step. A period of irregularity follows, as shown in the second panel for* $t = 185$ *to* 199. *For* $t = 185$ *to* 188, *the time series still appears regular, but we see from state space that the orbit is oscillating near the basin boundary. This leads to a visitation of the unstable equilibrium beginning at* $t = 189$, *and the orbit lingers there before moving away. The move away is shown in the third panel with* $t = 199$ *to* 214 *as the system regains regularity. The fourth panel,* $t = 214$ *to* 225, *is fairly regular, deviating minimally from the* 4*-cycle pattern. The fifth panel of the time series,* $t = 225$ *to* 235, *shows the stochastic orbit landing inside the* 10% *zone at* $t = 226$, *and again at* $t = 227$, *after which a phase change occurs. With the phase change comes a new period of irregularity, as the stochastic orbit is knocked far from the attractor before finally returning to the* 4*-cycle for the last few time steps. The last panel shows a close-up of the equilibrium visitation for* $t = 189$ *to* 199. *The unstable equilibrium is located at* $(v, h) = (100.80, 112.00)$, *within the diamond created by the* 50% *contour lines.*

where x_t and y_t are the numbers of juveniles and adults at time t, respectively, and b, α, and μ are positive constants with $0 < \mu < 1$. Here the random vector $\mathbf{E}_t = (E_{1t}, E_{2t})'$ is assumed to have bivariate normal distribution with mean vector $\mathbf{0}$. The deterministic Bartlett model obtains for $\mathbf{E}_t$ identically $\mathbf{0}$. When $b = 3.14$, $\alpha = 0.02$, and $\mu = 0.9$, the deterministic Bartlett model has a stable 4-cycle attractor [6]. See Figure 3.4(a). The 4-cycle attractor corresponds to four different stable solutions, one for each phase of the cycle. The corresponding four basins of attraction, along with the four values on the stable cycle, are shown in Figure 3.4(b). A repelling equilibrium exists at the vortex of the pinwheel of basin boundaries.

When noise is incorporated into the Bartlett model (3.3), the values of $P(x, y)$ can be computed numerically. Figure 3.4(c) shows 10% contours (blue) and 50% contours (red) in state space. While the 50% contours roughly follow the basin boundaries, there are regions (for example, inside the diamond around the repellor formed by the 50% contour) for which $P(x, y) > 50\%$. A 600 step stochastic simulation also is plotted in Figure 3.4(c). The majority of orbit points that give rise to a phase switch at the next time step (green diamonds) do fall within the 10% zone, as expected.

The 10% zones also warn of other types of cycle irregularities. Figure 3.5 shows a segment of the stochastic simulation in Figure 3.4(c), both as a time series and in state space. Two main periods of cycle irregularity occur during this segment. (A long period of damped oscillations begins at $t = 189$, and an "up-up-down-down" irregularity with large amplitude begins at $t = 227$.) Initially, the segment tends to follow the deterministic 4-cycle fairly closely. However, at $t = 185$ the orbit lands in a 10% zone, and a long episode of irregularity follows. Note that for $t = 185$ to 188, the time series in Figure 3.5(a) still appears regular, but we see from state space in Figure 3.5(b) that the orbit is oscillating near the basin boundary. This leads to a visitation of the unstable equilibrium beginning at $t = 189$, and the orbit lingers there for ten more time steps before moving away for $t = 199$ to 214. For $t = 214$ to 225, the system is fairly regular, deviating minimally from the 4-cycle pattern. The stochastic orbit lands inside the 10% zone at $t = 226$ and again at $t = 227$, after which a phase change occurs. With the phase change comes another period of irregularity, as the stochastic orbit is knocked far from the attractor before finally returning to the 4-cycle for the last few time steps of the segment. Note that the crucial orbit points themselves at $t = 185$ and $t = 226$ would seem unremarkable in the unfolding time series (Figure 3.5(a)) unless one realized they were sufficiently close to the basin boundaries to be in the 10% zones. A recognition, however, that they are in the 10% zones warns of the two impending episodes of cycle disruption.

4. Theory applied to experimental data. In this section, we apply our proposed rule of thumb for predicting cycle irregularities to experimental data.

The discrete stage-structured "LPA" *Tribolium* model has successfully explained and predicted nonlinear phenomena in a variety of contexts, including transitions between dynamic regimes (such as equilibria, 2-cycles, 3-cycles, invariant loops, and chaos), multiple attractors, saddle influences, stable and unstable manifolds, and lattice effects [4, 7, 5, 10, 8, 11, 12, 9, 13, 14, 15, 17, 18, 28, 24, 27, 25, 26, 30]. We now use the LPA model and the methods proposed in this paper to predict the cycle irregularities observed by Desharnais and Costantino [16].

Noise in laboratory cultures of flour beetles is mainly demographic [15]. A version of the

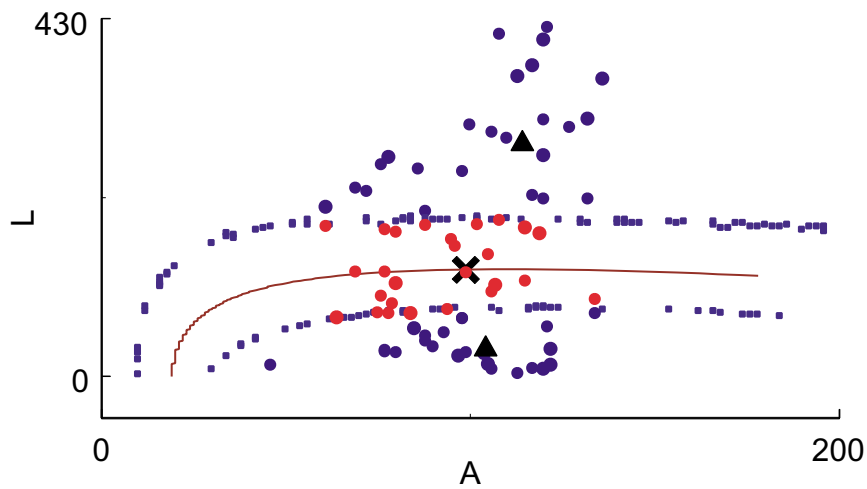

Figure 4.1. *Experimental data shown in cross section of state space at $P = 30$ for LPA model. The red curve shows the location of the basin boundary as calculated by the deterministic model. The blue curves bracket the 10% zones. Here $\sigma_l = 3.848$, $\sigma_p = 2.962$, and $\sigma_a = .2401$. Experimental data control replicates A,B,C, and D from Desharnais and Costantino [16] are projected onto the plane $P = 30$. Data points which fall within the 10% zone are shown in red. Projections of the 2-cycle coordinates $(L, P, A) = (35.26, 136.26, 104.14)$, $(282.24, 17.03, 114.08)$, and the unstable equilibrium $(L, P, A) = (128.03, 61.83, 98.74)$ are indicated by black triangles and a black "x," respectively.*

LPA model incorporating demographic stochasticity is

$$
\begin{aligned}
L_{t+1} &= \left(\sqrt{bA_t \exp\left(-c_{el}L_t - c_{ea}A_t\right)} + E_{1t}\right)^2, \\
P_{t+1} &= \left(\sqrt{(1-\mu_l)\,L_t} + E_{2t}\right)^2, \\
A_{t+1} &= \left(\sqrt{P_t \exp\left(-c_{pa}A_t\right) + (1-\mu_a)\,A_t} + E_{3t}\right)^2,
\end{aligned}
\tag{4.1}
$$

where L denotes the number of (feeding) larvae, P denotes the number of pupae (nonfeeding larvae, pupae, and callow adults), and A denotes the number of (mature) adults. The discrete time interval is two weeks. The coefficient $b > 0$ denotes the average number of larvae recruited per adult per unit time in the absence of cannibalism, μ_l and μ_a are the larval and adult per unit time probabilities of dying from causes other than cannibalism, and the exponentials represent the probabilities that individuals survive cannibalism one unit of time, with "cannibalism coefficients" c_{el}, c_{ea}, $c_{pa} > 0$. The random vector $\mathbf{E}_t = (E_{1t}, E_{2t}, E_{3t})'$ is assumed to have trivariate normal distribution with mean vector $\mathbf{0}$ and variance-covariance matrix $\mathbf{\Sigma}_{LPA}$. $\mathbf{E}_0$, $\mathbf{E}_1$, ... are assumed to be uncorrelated. The deterministic skeleton ($\mathbf{\Sigma}_{LPA} = \mathbf{0}$) of model (4.1) is the deterministic LPA model. Local stability results for the LPA model are obtained using standard linearization techniques [8, 23].

The conditioned least squares parameter estimates from the four control replicates reported in Desharnais and Costantino [16] were $b = 8.913$, $c_{el} = 0.008446$, $c_{ea} = 0.008572$,

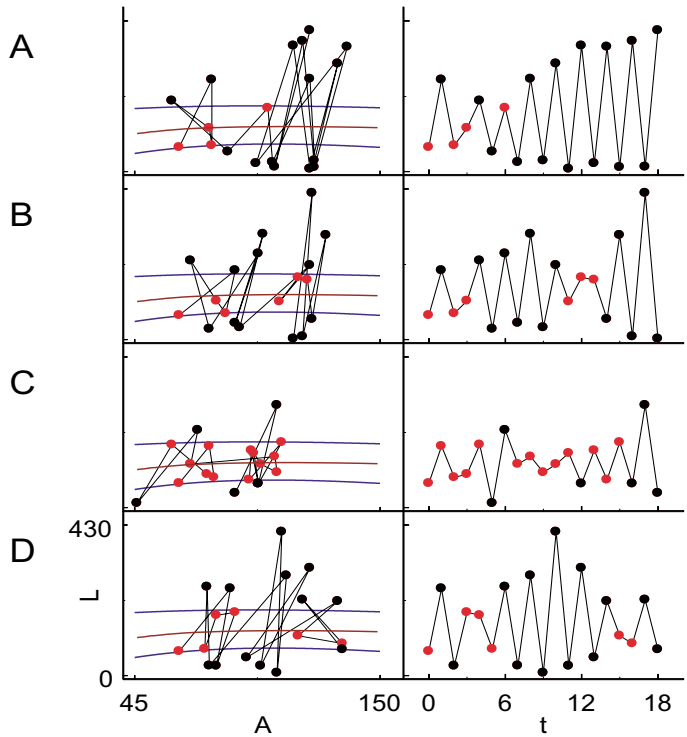

Figure 4.2. *Experimental data control replicates A,B,C, and D from Desharnais and Costantino* [16]*. The panels on the left show the cross-section of LPA state space at* $P = 30$*. Red and blue curves indicate the basin boundary and the* 10% *contours, respectively. Red data points are those within the* 10% *zones. The time series (L versus t) of the replicates are shown on the right. The time series illustrates how most cycle irregularities can be predicted by the* 10% *zone rule. Note the saddle fly-by in replicate C.*

$\mu_l = 0.5171$, $c_{pa} = 0.01795$, and $\mu_a = 0.1064$, with

$$\mathbf{\Sigma}_{LPA} = \begin{pmatrix} 3.848 & 0.3665 & 0.1440 \\ 0.3665 & 2.962 & -0.5895 \\ 0.1440 & -0.5895 & 0.2401 \end{pmatrix}.$$

At these parameter values, the deterministic LPA model admits an unstable saddle point (rounded to the nearest beetle) of $[128, 62, 99]$. The LPA model also predicts a 2-cycle attractor and hence two stable 2-cycle solutions (one for each phase of the cycle). The basins of attraction for these phases, along with the replicate data, are shown in Figure 4.1. The red curve is the basin boundary, and the blue curves are the 10% contours. The red data points lie within the 10% zone. The two values of the 2-cycle are shown, as well as the saddle, which lies on the basin boundary.

Figure 4.2 presents each replicate both in state space and as a time series. From the time series, it is clear that all cycle irregularities were preceded by a data point falling into the 10% zone. Of course, not all visitations of the 10% zone actually led to cycle disturbances.

5. Summary and discussion. Populations often exhibit temporal cycles, but as a result of noise, the oscillations may display irregularities in phase and amplitude. Understanding and anticipating such irregularities is of great importance in applications from pest control and species conservation to physiology and epidemiology [35]. In this paper, we have proposed a method for understanding and predicting cycle irregularities. The method is model-based. It requires a deterministic model for the population dynamics, together with a stochastic version of the model that describes random deviations from the deterministic predictions. If the deterministic model is autonomous, each phase of the cycle attractor is a stable solution. For each phase there is a basin of attraction, and these basins are separated by basin boundaries which may contain unstable equilibria. In general, the closer to the basin boundary a data point falls, the higher the probability it will stochastically switch phase at the next time step. Amplitude-dampened oscillations, caused by saddle fly-bys or repellor visitations, also occur when the data fall near the basin boundary, since that is where the unstable equilibria lie and exert the most influence. The probability $P(x)$ of phase switching at the next time step, given the current position x, can be computed with the stochastic model. "Warning zones" can be constructed in state space by computing contour lines along which $P(x)$ is constant. These zones follow and contain the basin boundaries. When data fall within the warning zones, the observer is informed that a cycle irregularity is likely to occur and can act accordingly. In this paper, we have defined the warning zones using the 10% contours, i.e., where a greater than 10% chance of phase switching is predicted. A more conservative approach would use a smaller contour value (and hence a wider zone around the basin boundaries). The actual contour value chosen is subjective and depends on the acceptable risk level in the particular application.

Dynamical systems approaches are powerful tools for understanding biological systems. Situation specific applications of model-based methods, including the one presented in this paper, require constructing a model in whose accuracy one has confidence. During the last few decades, rigorous connection of mathematical models with population data has become possible for several laboratory systems (see, for example, Bjørnstad and Grenfell [2], Cushing et al. [9], Fussmann et al. [21], and the references cited in section 4), but quantitatively accurate models for field populations are still rare [29]. Until reliable models become more common and established in ecology, there will be a need for nonparametric methods. An interesting and important open question is whether nonparametric versions of the method presented in this paper can be constructed when good data but no structural models are available.

Acknowledgments. We thank R. F. Costantino, Brian Dennis, and R. A. Desharnais as well as two anonymous referees.

REFERENCES

[1] M. S. Bartlett, *Stochastic Population Models*, Wiley, New York, 1960, p. 50.

[2] O. N. Bjørnstad and B. T. Grenfell, *Noisy clockwork: Time series analysis of population fluctuations in animals*, Science, 293 (2001), pp. 638–643.

[3] C. J. Briggs, S. M. Sait, M. Begon, D. J. Thompson, and H. C. J. Godfray, *What causes generation cycles in populations of stored-product moths?*, J. Animal Ecol., 69 (2000), pp. 352–366.

[4] R. F. Costantino, J. M. Cushing, B. Dennis, and R. A. Desharnais, *Experimentally induced transitions in the dynamic behavior of insect populations*, Nature, 375 (1995), pp. 227–230.

[5] R. F. Costantino, J. M. Cushing, B. Dennis, R. A. Desharnais, and S. M. Henson, *Resonant population cycles in alternating habitats*, Bull. Math. Biol., 60 (1998), pp. 247–273.

[6] R. F. Costantino and R. A. Desharnais, *Population Dynamics and the* Tribolium *Model: Genetics and Demography*, Springer-Verlag, New York, 1991.

[7] R. F. Costantino, R. A. Desharnais, J. M. Cushing, and B. Dennis, *Chaotic dynamics in an insect population*, Science, 275 (1997), pp. 389–391.

[8] J. M. Cushing, R. F. Costantino, B. Dennis, R. A. Desharnais, and S. M. Henson, *Nonlinear population dynamics: Models, experiments, and data*, J. Theor. Biol., 194 (1998), pp. 1–9.

[9] J. M. Cushing, R. F. Costantino, B. Dennis, R. A. Desharnais, and S. M. Henson, *Chaos in Ecology: Experimental Nonlinear Dynamics*, Academic Press, San Diego, 2003.

[10] J. M. Cushing, B. Dennis, R. A. Desharnais, and R. F. Costantino, *An interdisciplinary approach to understanding nonlinear ecological dynamics*, Ecol. Model., 92 (1996), pp. 111–119.

[11] J. M. Cushing, B. Dennis, R. A. Desharnais, and R. F. Costantino, *Moving toward an unstable equilibrium: Saddle nodes in population systems*, J. Animal Ecol., 67 (1998), pp. 298–306.

[12] J. M. Cushing, S. M. Henson, R. A. Desharnais, B. Dennis, R. F. Costantino, and A. A. King, *A chaotic attractor in ecology: Theory and experimental data*, Chaos Solitons Fractals, 12 (2001), pp. 219–234.

[13] B. Dennis, R. A. Desharnais, J. M. Cushing, and R. F. Costantino, *Nonlinear demographic dynamics: Mathematical models, statistical methods, and biological experiments*, Ecol. Monogr., 65 (1995), pp. 261–281.

[14] B. Dennis, R. A. Desharnais, J. M. Cushing, and R. F. Costantino, *Transitions in population dynamics: Equilibria to periodic cycles to aperiodic cycles*, J. Animal Ecol., 66 (1997), pp. 704–729.

[15] B. Dennis, R. A. Desharnais, J. M. Cushing, S. M. Henson, and R. F. Costantino, *Estimating chaos and complex dynamics in an insect population*, Ecol. Monogr., 71 (2001), pp. 277–303.

[16] R. A. Desharnais and R. F. Costantino, *Genetic analysis of a population of Tribolium.* VII. *Stability: Response to genetic and demographic perturbations*, Can. J. Genet. Cytol., 22 (1980), pp. 577–589.

[17] R. A. Desharnais, R. F. Costantino, J. M. Cushing, and B. Dennis, *Estimating chaos in an insect population*, Science, 276 (1997), pp. 1881–1882.

[18] R. A. Desharnais, R. F. Costantino, J. M. Cushing, S. M. Henson, and B. Dennis, *Chaos and population control of insect outbreaks*, Ecol. Let., 4 (2001), pp. 229–235.

[19] R. A. Desharnais and L. Liu, *Stable demographic limit cycles in laboratory populations of* Tribolium castaneum, J. Animal Ecol., 56 (1987), pp. 885–906.

[20] L. Edelstein-Keshet, *Mathematical Models in Biology*, McGraw–Hill, Boston, 1988, p. 105.

[21] G. F. Fussmann, S. P. Ellner, K. W. Shertzer, and N. G. Hairston, *Crossing the Hopf bifurcation in a live predator-prey system*, Science, 290 (2000), pp. 1358–1360.

[22] G. F. Gause, *The Struggle for Existence*, Hafner Publishing Company, New York, 1964, p. 144.

[23] J. Guckenheimer and P. Holmes, *Nonlinear Oscillations, Dynamical Systems, and Bifurcations of Vector Fields*, Springer-Verlag, Berlin, 1983.

[24] S. M. Henson, R. F. Costantino, J. M. Cushing, B. Dennis, and R. A. Desharnais, *Multiple attractors, saddles, and population dynamics in periodic habitats*, Bull. Math. Biol., 61 (1999), pp. 1121–1149.

[25] S. M. Henson, R. F. Costantino, R. A. Desharnais, J. M. Cushing, and B. Dennis, *Basins of attraction: Population dynamics with two locally stable* 4*-cycles*, Oikos, 98 (2002), pp. 17–24.

[26] S. M. Henson and J. M. Cushing, *The effect of periodic habitat fluctuations on a nonlinear insect population model*, J. Math. Biol., 36 (1997), pp. 201–226.

[27] S. M. Henson, R. F. Costantino, J. M. Cushing, R. A. Desharnais, B. Dennis, and A. A. King, *Lattice effects observed in chaotic dynamics of experimental populations*, Science, 294 (2001), pp. 602–605.

[28] S. M. Henson, J. M. Cushing, R. F. Costantino, B. Dennis, and R. A. Desharnais, *Phase switching in population cycles*, Proc. Roy. Soc. London Ser. B, 265 (1998), pp. 2229–2234.

[29] S. M. Henson, J. L. Hayward, C. M. Burden, C. J. Logan, and J. G. Galusha, *Predicting the dynamics of aggregate loafing behavior in gulls*, The Auk, submitted, 2003.

[30] A. A. King, R. A. Desharnais, S. M. Henson, R. F. Costantino, J. M. Cushing, and B. Dennis, *Random perturbations and lattice effects in chaotic population dynamics*, Science, 297 (2002), p. 2163a.

[31] R. M. May, *Biological populations with nonoverlapping generations: Stable points, stable cycles, and chaos*, Science, 186 (1974), pp. 645–647.

[32] P. A. P. Moran, *Some remarks on animal population dynamics*, Biometrics, 6 (1950), pp. 250–258.

[33] A. J. Nicholson, *The self-adjustment of populations to change*, Cold Spring Harbor Symposia on Quantitative Biology, 22 (1957), pp. 153–173.

[34] W. E. Ricker, *Stock and recruitment*, J. Fish. Res. Bd. Can., 11 (1954), pp. 559–623.

[35] W. M. Schaffer, B. E. Kendall, C. W. Tidd, and L. F. Olsen, *Transient periodicity and episodic predictability in biological dynamics*, IMA J. Math. Appl. Med. Biol., 10 (1993), pp. 227–247.

[36] H. Tong, *Nonlinear Time Series: A Dynamical System Approach*, Oxford University Press, Oxford, UK, 1990.

[37] S. Utida, *Population fluctuations, an experimental and theoretical approach*, Cold Spring Harbor Symposia on Quantitative Biology, 22 (1957), pp. 139–151.